Electronic Structure of Silicon Nitride according to ab initio Quantum-Chemical Calculations and Experimental Data

S. S. Nekrashevich[a], V. A. Gritsenko[a], R. Klauser[b], and S. Gwo[c]

[a]*Institute of Semiconductor Physics, Siberian Branch, Russian Academy of Sciences, Novosibirsk, 630090 Russia*
[b]*Synchrotron Radiation Research Center, Taiwan, Republic of China*
[c]*Department of Physics, National Tsing-Hua University, Taiwan, Republic of China*
e-mail: nss@isp.nsc.ru
Received March 25, 2010

Abstract—Charge transfer $\Delta Q = 0.35e$ at the Si−N bond in silicon nitride is determined experimentally using photoelectron spectroscopy, and the ionic formula of silicon nitride $Si_3^{+1.4}N_4^{-1.05}$ is derived. The electronic structure of α-Si_3N_4 is studied ab initio using the density functional method. The results of calculations (partial density of states) are compared with experimental data on X-ray emission spectroscopy of amorphous Si_3N_4. The electronic structure of the valence band of amorphous Si_3N_4 is studied using synchrotron radiation at different excitation energies. The electron and hole effective masses $m_e^* \approx m_h^* \approx 0.5m_e$ are estimated theoretically. The calculated values correspond to experimental results on injection of electrons and holes into silicon nitride.

1. INTRODUCTION

Amorphous silicon oxide (SiO_2) and nitride (Si_3N_4) are two basic dielectrics in devices operating on silicon integrated circuits. These dielectrics have permitted astounding progress in semiconductor silicon electronics, which has replaced vacuum electronics. Silicon oxide has a low density of states at the silicon−dielectric interface, a high breakdown field, and a low trap concentration. This dielectric is used as a gate insulator in metal−insulator−semiconductor (MIS) transistors. Silicon nitride has a much higher concentration of electron and hole traps (about 10^{19} cm^{-3}) as compared to silicon oxide [1, 2]. Traps in Si_3N_4 are deep ($W \approx 1.5$ eV) [3]. Silicon nitride exhibits the memory effect, viz., the ability to localize (trap) electrons and holes injected into it with a giant lifetime in the localized state (about 10 years at $T = 85°C$) [2]. The memory effect in silicon nitride is used in developing nonvolatile flash-memory effects (storing information without a power supply) in flash memory devices [4−6]. Amorphous silicon nitride is used in electronic devices.

Silicon nitride in the crystalline state is used as a ceramic with high hardness, wear resistance (it is used in cutting tools), strength, heat resistance, and a low relative density (it is used in human bone prosthetics).

The mechanical, optical, and electrical properties of silicon nitride are determined by its electronic structure. In recent years, considerable advances have been made in understanding the electronic structure of wide-band-gap solids owing to progress in computational technique and the development of complex ab initio programs for simulating the electronic structure of solids. The electronic structure of crystalline silicon nitride was studied theoretically in [7−10]. In the crystalline state, silicon nitride exists in the α and β phases. The low-temperature α phase passes to the energetically more advantageous β phase at a temperature of 1723°C. The lattices of the α and β phases of silicon nitride possess hexagonal symmetry. The short-range order is determined by the tetrahedral surroundings of the silicon atom in SiN_4. Nitrogen (N) atoms are coordinated with three silicon atoms lying in approximately the same plane.

In [7, 10], the electronic band structure of α and β phases of silicon nitride was calculated using the ab initio method. The authors of [7, 10] noted that the band structures of both phases are very close and the main properties of the electronic structure are determined almost completely by the short-range order. From the point of view of atomic structure, the α phase is the closest to amorphous nitride Si_3N_4 [1, 11]. The calculated value of the electron effective mass lies in the range $m_e^* = (0.19−0.63)m_0$. This value is in good agreement with the experimental value of the electron tunneling effective mass $m_e^* = (0.4−0.6)m_0$ in amorphous silicon nitride [12−18]. The situation with the hole effective mass is different. Experiments on tunnelling injection of holes into amorphous Si_3N_4 indicate that the contribution to the tunnel effect
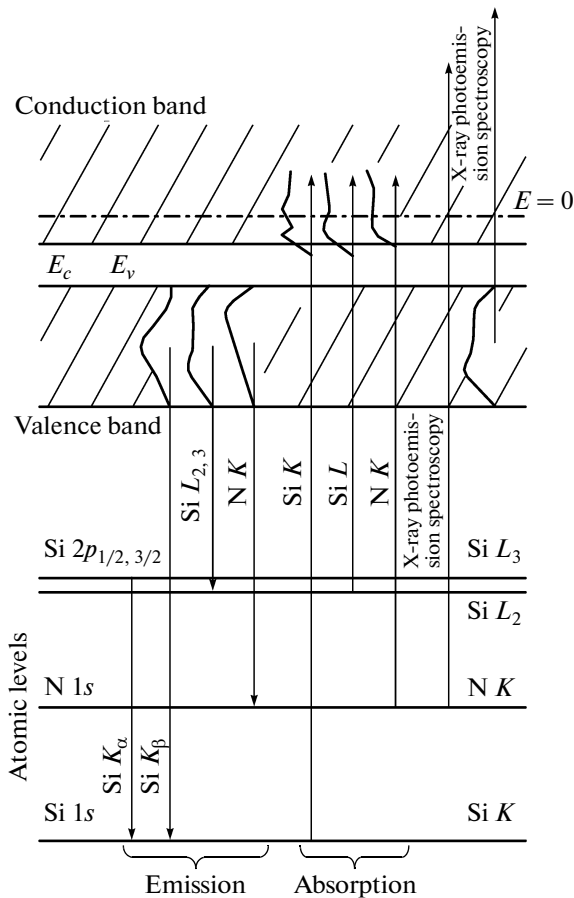
Conduction band

$E = 0$

E_c E_v

Valence band

X-ray photoemis-sion spectroscopy

Si $L_{2,3}$ N K Si K Si L N K X-ray photoemis-sion spectroscopy

Si $2p_{1/2, 3/2}$

Si L_3

Si L_2

Atomic levels

N $1s$

N K

Si K_α Si K_β

Si $1s$

Si K

Emission   Absorption

Fig. 1. Diagram of electron transitions observed in experiments of X-ray emission spectroscopy, X-ray absorption spectra, and X-ray photoelectron spectroscopy. Horizontal lines denote atomic level, vertical arrows indicate electron transitions.

comes from light holes with m_h^* $(0.35-0.50)m_0$ [13, 17–19]. At the same time, band calculations predict the presence of heavy holes with $m_h^* \approx (2.5-3.7)m_0$ [7]. In [8], light holes with mass $m_h^* \approx 0.55m_0$ were detected in α-Si$_3$N$_4$. However, the charge transfer at the Si−N bond calculated in [8] had an anomalously large value of $\Delta Q = 0.63e$ as compared to the results of later calculations ($\Delta Q = 0.31e$) [10]. Reliable data on the effective masses of electrons and holes in silicon nitride are important because flash memory is reprogrammed on the basis of silicon nitride due to tunneling injection. The injection rate is an exponential function of the effective mass [6]. The aim of this study is an experimental and theoretical analysis of the electronic structure of silicon nitride, calculation of the electron and hole effective masses using a contemporary ab initio method, and comparison of the results of calculations with the results of experiment performed, in particular, using synchrotron radiation.

2. EXPERIMENT

Amorphous Si$_3$N$_4$ samples about 5 nm in thickness were obtained by pyrolysis of a mixture of dichlorsilane (SiH$_2$Cl$_2$) and ammonia NH$_3$ in a low-pressure reactor at 760°C. The substrates were n-type silicon plates with the (100) orientation and a resistivity of about 10 Ω cm. X-ray and UV photoelectron spectra were measured on a Kratos AXIS-HS spectrometer with a high (0.25 eV) resolution. The spectra were measured under excitation by monochromatized K_α radiation of Al with an energy of 1486.6 eV. The UV spectra were measured on the He II line with an energy of 40.8 eV. Photoelectrons were detected at an angle of 60° to the normal to the sample surface.

Photoelectron spectra of the valence band of amorphous Si$_3$N$_4$ with different excitation energies (200, 384, 620, and 1000 eV) were detected under excitation by synchrotron radiation from the accelerator at the National Synchrotron Radiation Research Center (Hsinchu, Taiwan). The experimental technique is described in [20].

The energy level diagram of the experiments used for Si$_3$N$_4$ spectroscopy is shown in Fig. 1. Information on the partial density of states in the valence band was obtained using experimental X-ray emission spectra. The experiments are based on recording the emission spectra formed as a result of filling of vacant states (holes) by electrons at the atomic core levels $1s$, $2p$ in silicon and $1s$ of nitrogen. The intensity of X-rays is proportional to the density of electron states in the valence band. The width of the valence band in Si$_3$N$_4$ is about 13 eV, which is much smaller than the energy of the X-ray transitions observed in the emission spectra. For this reason, we assume that the matrix element of the transition depends on energy only slightly. In the dipole approximation, X-ray transitions in which the orbital angular momentum changes by ±1 are allowed. In accordance with the dipole selection rules, the emission spectra for silicon exhibit transitions from the $3s$ and $3d$ states in the valence band to the $2p$ atomic level ($L_{2, 3}$ level in the notation used in X-ray spectroscopy). The K emission spectra of silicon exhibit transitions from the $3p$ states of the valence band to the $1s$ atomic level.

The density of states in the conduction band is analyzed with the help of X-ray absorption spectra, or quantum yield spectra (QYS). In the QYS, transitions from the filled atomic $1s$ and $2p$ levels of silicon and $1s$ level of nitrogen to unfilled vacant states in the conduction band are detected. The QYS in the first approximation are interpreted in the approximation of the dipole selection rules.

3. METHODS OF QUANTUM-CHEMICAL CALCULATIONS

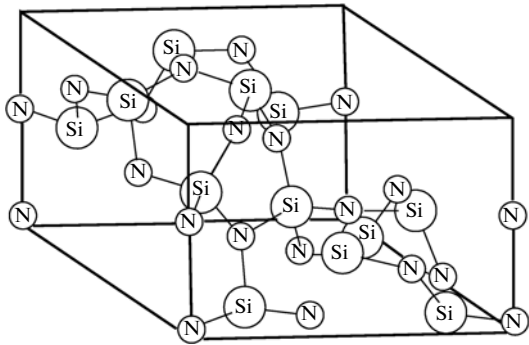Band calculations of the electronic structure were performed using the Quantum-Espresso software

Fig. 2. Unit cell of α-Si$_3$N$_4$.

package [21] based on the density functional theory (DFT): planes waves and pseudopotentials are used as the basis for ab initio computation. The periodic structure of the crystal is taken into account in terms of the boundary conditions at the unit cell boundary.

In our calculations, we used the following electronic configurations for Si: [Ne] $3S^2\,3P^2\,3D^0$ and for N: [He] $2S^2\,2P^3$. These states corresponded to the valence shells, while [Ne] and [He] corresponded to the core. The core electrons were taken into account using ultrasoft pseudopotentials. We employed a nonlocal exchange-correlated functional in the Perdew−Burke−Ernzerhof (PBE) parameterization. The cutoff energy for plane waves in self-consistent calculations was chosen so that the resultant convergence in the total energy of the cell was not worse than 0.001 Ry/at and the total energy was 45 Ry. The density of the k-point mesh in the reciprocal space in self-consistent calculations was chosen from the same considerations.

The effective masses of electrons and holes were estimated numerically from the resultant set of $E(k)$ points in the Brillouin zone by approximating the dispersion curve by a parabola in the vicinity of a local extremum. To determine the positions of extremal points (top of the valence band and the bottom of the conduction band) exactly and to obtain a high-density discrete mesh in the vicinity of the extrema, additional non-self-consistent calculations were performed using the potentials obtained in the preceding self-consistent calculation.

4. ELECTRONIC STRUCTURE OF α-Si$_3$N$_4$ AND COMPARISON WITH EXPERIMENT ON AMORPHOUS SILICON NITRIDE

The unit cell in α-Si$_3$N$_4$ (Fig. 2) belongs to the trigonal system ($a = b = 7.751$ Å, $c = 5.619$ Å, $\alpha = \beta = 90°$, $\gamma = 120°$) and contains 28 atoms (12 silicon atoms and 16 nitrogen atoms) [2]. The average values of the Si−N−Si angles in α-Si$_3$N$_4$ α-Si$_3$N$_4$ are 118°8′. The length of the Si−N bond in crystalline silicon nitride is in the range 1.707−1.779 Å [11]. The Si−Si spacing in

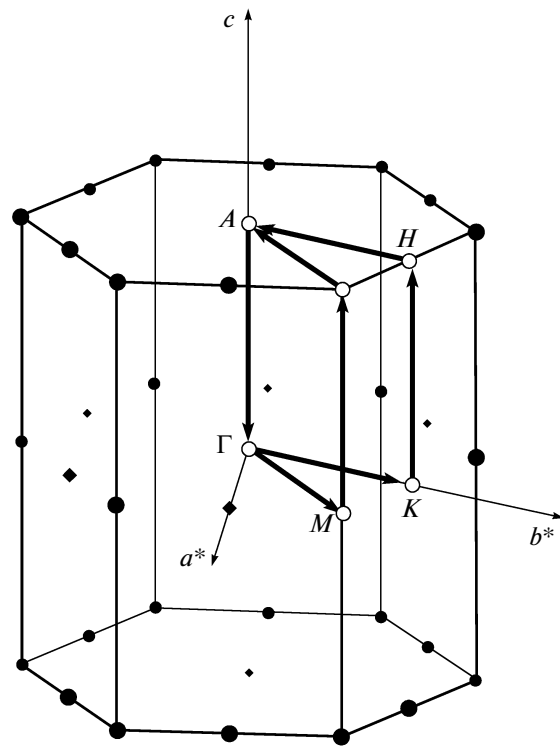**Fig. 3.** Brillouin zone of α-Si$_3$N$_4$.

the second coordination sphere is close to 3.0 Å, while the N−N distance is in the range 2.67−2.90 Å. The unit cell parameters were taken from the ICSD crystallographic database [22].

Figure 3 shows the first Brillouin zone corresponding to the unit cell of α-Si$_3$N$_4$ with high-symmetry points and with the path traversed through these points in the opposite direction, along which the band structure was calculated. The calculated band structure of the α phase of silicon nitride is shown in Fig. 4 (the energy is measured from the top of the valence band).

Analysis of the resultant band structure shows that α-Si$_3$N$_4$ is a non-direct-band insulator with the top of the valence band at point M and the bottom of the conduction band at the center of the Brillouin zone. The valence band of silicon nitride is formed by two subbands separated by an ionic gap with a width of about 4 eV. The calculated band gap is $E_g = 4.66$ eV, which is in good agreement with the experimental value (4.5 eV) [2]. The resultant dispersion relation

Effective masses of charge carriers in α-Si$_3$N$_4$

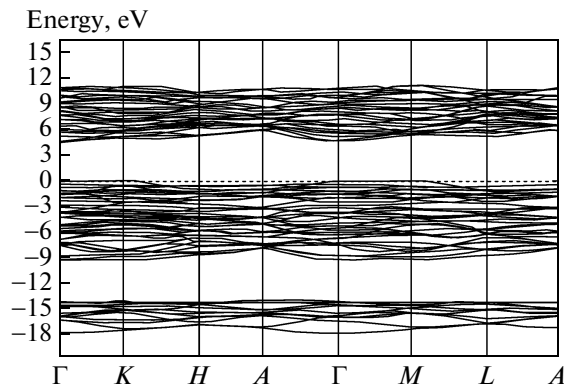|	Light	Heavy
m_e^*/m_0	0.75 ($G–A$)	1 ($G–K$, $G–M$)
m_h^*/m_0	0.43 ($M–L$)	~25 ($M–G$, $M–K$)

Energy, eV

Fig. 4. Dependence of energy on quasi-momentum in α-Si_3N_4.

$E(\mathbf{k})$ has made it possible to calculate the effective masses of electrons and holes (see table).

The table contains the minimal and maximal values of the effective masses of electrons and holes and the corresponding directions in the reciprocal space. An anomalously high value of the effective mass (approximately $25m_0$) was obtained for holes in the G–K–M plane perpendicular to the hexagonal prism axis in the Brillouin zone, while a hole with a mass of $0.43m_0$ is observed in the direction parallel to the axis. The value of the effective mass of a light hole is in good agreement with the experimental value of the tunneling effective mass of a hole in amorphous silicon nitride, which is approximately $(0.35-0.50)m_0$ [13].

We have calculated and analyzed the spatial distributions of the electron density as a function of energy. Figure 5 shows the charge density distributions for three difference energies of the valence band. Figure 5a shows the charge density distributions in an energy range of -17 eV corresponding to $2s$ orbitals of nitrogen. In accordance with basic quantum-mechanical concepts, the obtained pattern of the electron density distribution has a symmetry close to spherical, which is typical of the wavefunctions of s electrons. Figure 5b shows the charge distribution for an energy

of -4 eV corresponding to the bonding orbital $2p$-Si sp in N. It can be seen from this pattern that α-Si_3N_4 is a polar crystal; the electron density at the Si–N bond is mainly localized near the nitrogen atom due to its high negative charge. The charge density gradient is directed along Si–N bonds, indicating the bonding nature of the orbital. Figure 5c shows the constant-electron-density surface for unbonding $2p_\pi$ orbitals of nitrogen (with an energy of -0.1 eV), from which the top of the valence band is formed [23, 24]. As expected, the wavefunction of the unbonding orbital is localized along the axis perpendicular to the plane formed by the nitrogen atom and its nearest neighbors (three silicon atoms).

Figure 6 shows the experimental X-ray emission spectra and quantum yield (absorption) spectra of amorphous Si_3N_4 borrowed from [25], as well as the calculated partial density of states for α-Si_3N_4. Except for the $L_{2,3}$ spectra of Si, satisfactory agreement is observed between experiment and theory. The absence of the second peak at the top of the valence band in the $L_{2,3}$ spectra of Si can be explained by the disregard for the contribution from $3d$ orbitals of Si, according to [26], which make a considerable contribution to the emission spectra.

5. ENERGY DIAGRAM OF ELECTRONIC TRANSITIONS IN AMORPHOUS Si_3N_4

Figure 7 shows the energy diagram of electron states in α-Si_3N_4. All energies are measured from the electron energy in vacuum. The energies of internal $2p$ and $2s$ levels in silicon and $1s$ level in nitrogen were determined using X-ray photoelectron spectroscopy; the energy of the $1s$ level of silicon is determined from the K_α emission spectrum of silicon, in which transitions between $2p$ and $1s$ levels of silicon are detected. The energy of this transition in Si_3N_4 is 1740.5 eV [1]. The horizontal lines in the valence band and in the conduction band in Fig. 7 correspond to the position of the peaks of the density of states observed in X-ray transitions. The figure shows the electron transitions observed in the X-ray emission and absorption spectra.
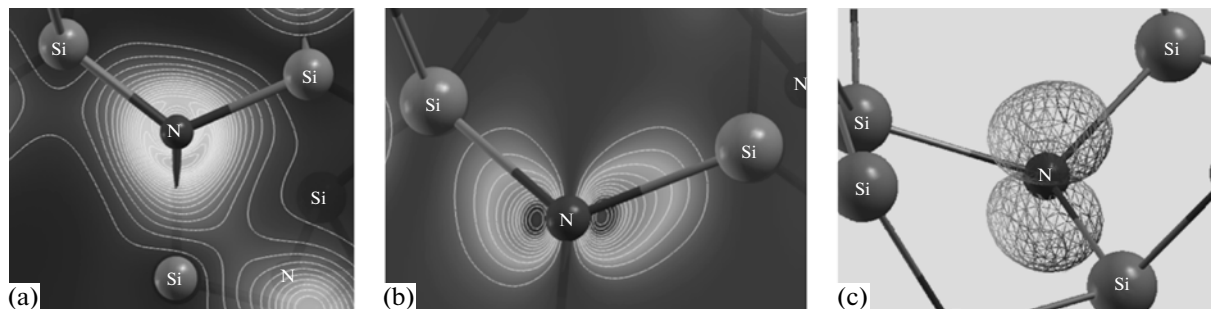

Fig. 5. Electron density distribution in α-Si_3N_4 at different energies: -17 (a), -4 (b), and -0.1 eV (c). The energy is measured from the top of the valence band.

The same figure also shows the electron transitions observed in the ionization spectra of the $2p$ levels in Si and $1s$ levels in N, as well as interband transitions from the valence band to the conduction band borrowed from [27]. The low-energy edge of the quantum yield of the $L_{2,3}$ spectra of silicon gets into the band gap. The quantum yield (with an energy of 1844.4 eV) in the K spectra of silicon is also localized in the band gap. It also includes transitions observed in the ionization spectra at energies $E = 101.0$ and 104.0 eV upon excitation of the $2p$ level of Si, as well as transitions with energies $E = 390.8$ and 399.1 eV upon excitation of the $1s$ levels of N (see Fig. 7). These peaks cannot be explained in the framework of one-electron calculations disregarding defects and multielectron effects in silicon nitride. These features can be due either to multielectron or defects. Clarification of the nature of low-energy transitions in the quantum yield and ionization spectra requires further investigation.

It can be seen from Fig. 7 that the transitions at energies $E = 9.3$, 10.8, and 14.5 eV coincide with the energy gap between bonding and nonbonding states. The transition at energies of 6.8 and 12.5 eV poorly correlates with the density-of-states peaks that are manifested in the X-ray transition. The optical reflection spectra for Si_3N_4 exhibit only one singularity at an energy of 9.5 eV [28]. This energy is close to the energy of 9.3 eV observed in the excitation spectra. It should be emphasized that the energy diagram in Fig. 7 is empirical and is plotted using the approach developed for SiO_2 [29].

6. DETERMINATION OF CHARGE TRANSFER TO THE Si−N BOND IN Si_3N_4

The energies of the atomic levels (e.g., the position of the $2p$ level of Si in tetrahedral Si, Si_3N_4, and SiO_2) are determined by the effective charges at silicon atoms, which in turn are determined by the electron affinity of atoms surrounding the silicon atom. The effective charge of an atom is a concept not quite definite nor unambiguous. However, comparison of compounds in a series with different charges leads to qualitative conclusions concerning the extent of overlapping of wavefunctions and charge transfer to the bond. Figure 8 shows experimental photoelectron spectra of the $2p$ level of silicon in Si_3N_4 and SiO_2. The $2p$ level of silicon in Si_3N_4 is separated from the $2p$ level in Si by 2.9 eV. The $2p$ level of silicon in SiO_2 is separated from the $2p$ in Si by 4.2 eV. The difference in the energies of the level (chemical shift) is due to the fact that the electron density from the s- and p-orbitals of the silicon atom is shifted to the $2p$ and $2p$ levels of nitrogen and oxygen as a result of formation of Si−N and Si−O bonds in Si_3N_4 and SiO_2, respectively. Therefore, the silicon atom acquires a positive charge, while nitrogen and oxygen atoms acquire a negative charge. Due to the positive charge on the silicon atom in Si_3N_4 and SiO_2, the binding energy of the $2p$ level of Si increases
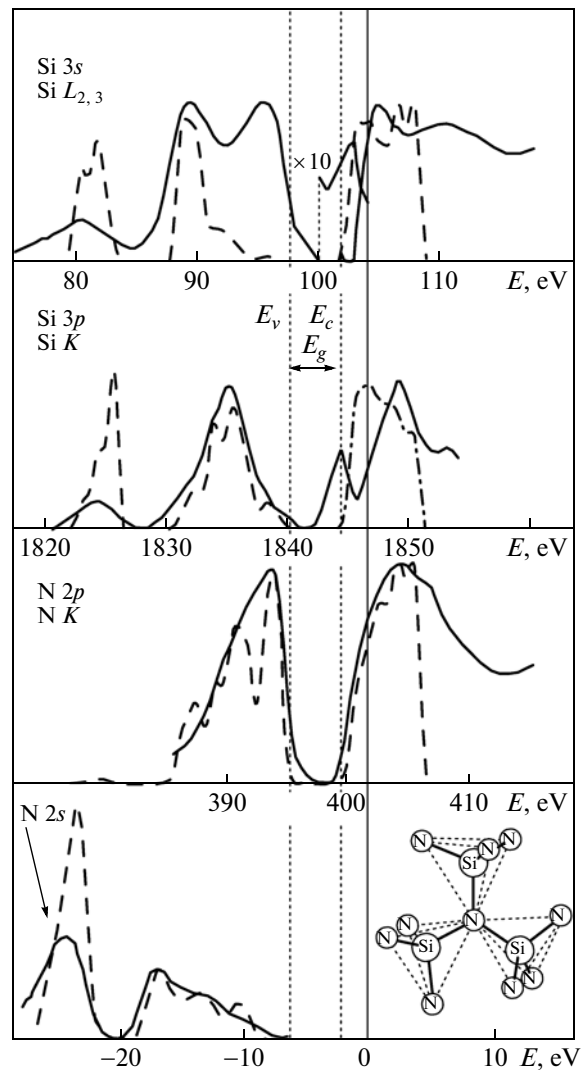

Fig. 6. Experimental X-ray emission spectra and quantum yield (absorption) spectra of amorphous Si_3N_4 (solid curves) and calculated partial density of states in α-Si_3N_4 (dashed curves). All spectra are reduced to the same origin, viz., electron energy in vacuum (solid vertical line). The X-ray photoelectron spectrum of the valence band is shown in the left bottom part for $E = 1486.6$ eV. Three tetrahedrons connected by a nitrogen atom are shown in the right bottom part of the figure.

because of the Coulomb interaction. This is the essence of the chemical shift of the $2p$ level of Si in Si_3N_4 and SiO_2 relative to Si in Fig. 8.

The charge on the oxygen atom in fused quartz, which was determined in experiments on annihilation of positrons, is $Q^0 = -1.0e$ [30]. Close values are obtained in theoretical quantum-chemical calculations of the electronic structure of SiO_2: $1.2e$ [31], $(1.02-1.3)e$ [32], $1.15e$ [33], and $1.2e$ [34]. Since the oxygen atom in SiO_2 is coordinated by two silicon atoms, the charge transfer at the Si−O bond amounts to $\Delta Q = 0.5e$. This means that SiO_2 is an ion−covalent compound with a large ionicity of the Si−O bond.
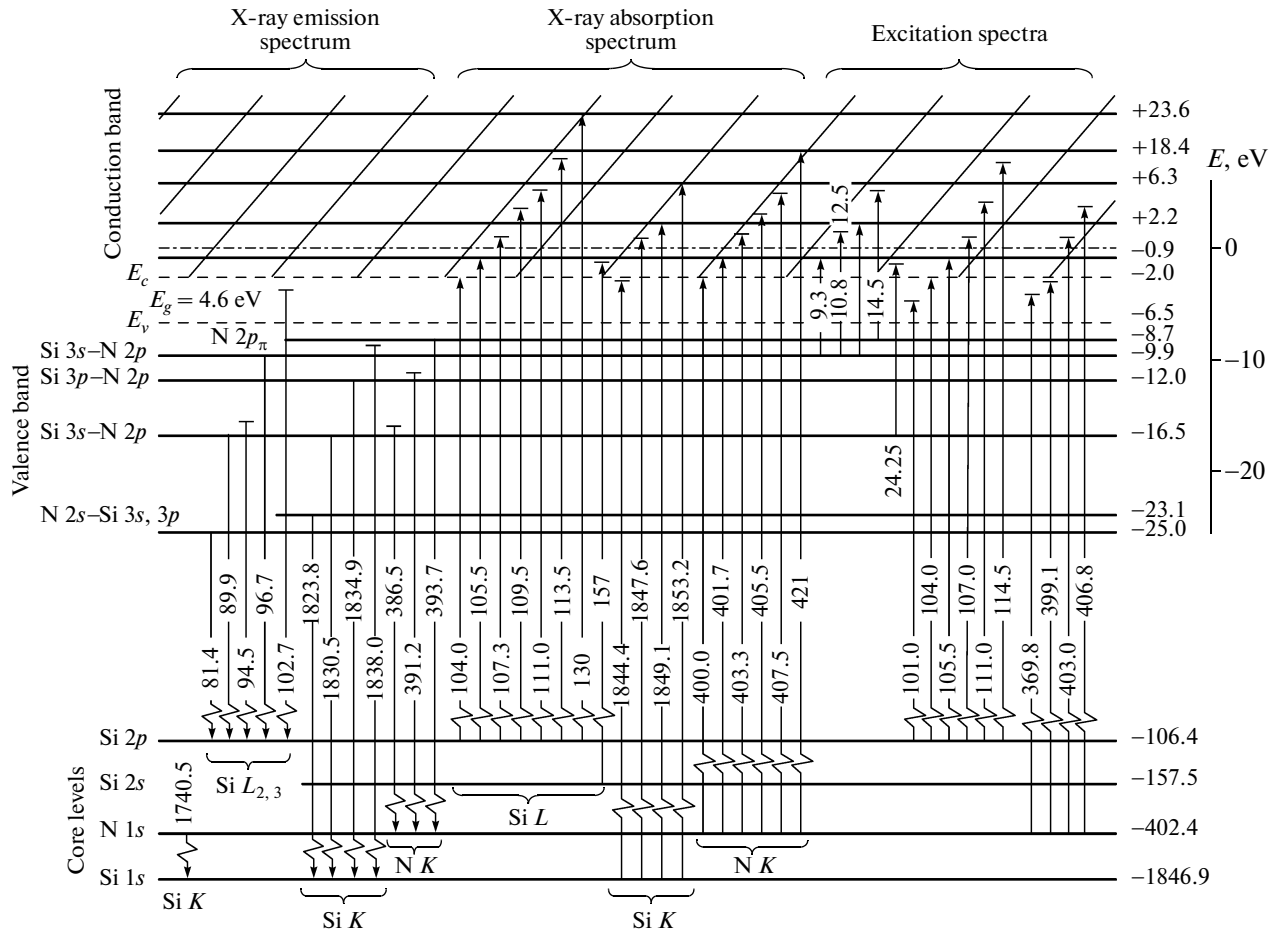
Fig. 7. Energy diagram of electron transitions in amorphous Si_3N_4. Horizontal lines denote the positions of atomic levels, as well as the positions of the peaks of the electron density of states in the valence band and in the conduction band; vertical arrows show electron transitions.

The chemical shift of the $2p$ level of Si in Fig. 8 makes it possible to determine the charge transfer at the Si–N bond in Si_3N_4. The Si–Si bond is purely covalent, and the charge at the silicon atom in elementary silicon is zero. If we assume, as is usually done, that the chemical shift of the $2p$ level of Si is prop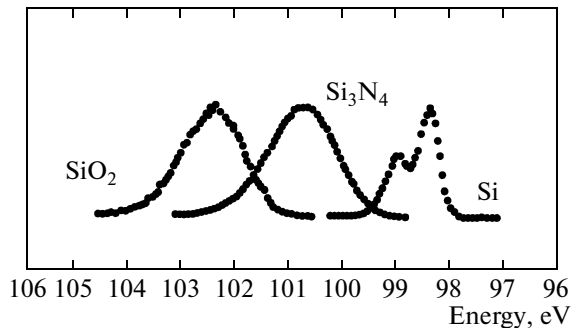ortional to the positive charge at the silicon atom, the charge on the Si atom in Si_3N_4 is $Q^{Si} = +1.4e$. Since the silicon atom in Si_3N_4 is coordinated by four nitrogen atoms, the charge transfer to the Si–N bond is $\Delta Q = 0.35e$. Since the nitrogen atom in Si_3N_4 is coordinated by three silicon atoms, the charge on the nitrogen atom is $Q^N = -1.05e$.

The experimentally determined charge transfer $\Delta Q = 0.35e$ to the Si–N bond is half the charge transfer of $0.7e$ calculated in [7]. The total charge calculated here for each species of atoms according to Luden ($Q^{Si} = +1.5e$, $Q^N = -1.0e$) has also made it possible to determine the charge transfer at the Si–N bond. The theoretically calculated charge transfer at the Si–N bond was $\Delta Q = 0.35 \pm 0.02e$. This value is in good agreement with the experimentally determined charge transfer.

Fig. 8. X-ray photoelectron spectra of the $2p$ level of the silicon atom in Si, Si_3N_4, and SiO_2.

7. PHOTOELECTRON SPECTRA OF THE VALENCE BAND

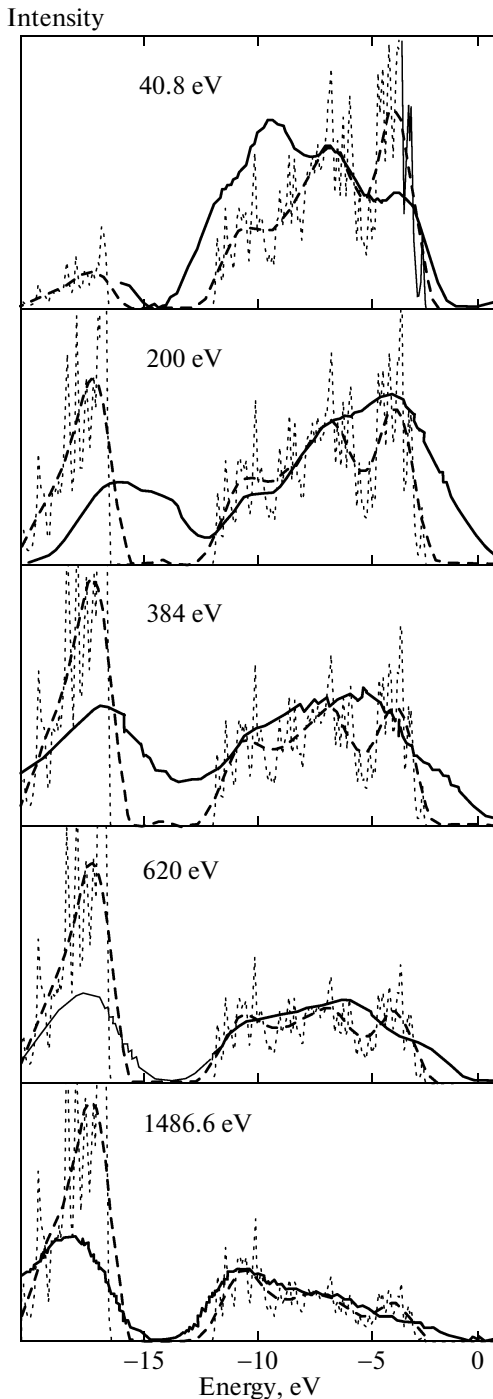Figure 9 shows the experimental photoelectron spectra of the valence band of amorphous Si_3N_4 mea-

Intensity

Fig. 9. Experimental and calculated photoelectron spectra of the valence band for amorphous Si_3N_4 with different excitation energies.

tions of the peaks on the experimental spectra are in satisfactory agreement with the model curves, but the peak intensity in the region of the 2s subband of N is overestimated in calculations for nearly all excitation energies. The reason for this discrepancy between experiment and calculations is unclear. Probably, the photoionization cross sections for 2s electrons in N were overestimated in theoretical calculations [35].

8. DISCUSSION OF RESULTS

Analysis shows that the upper valence band is formed by bonding orbitals 2p (N)−3sp^3 (Si). Unbonding $2p_\pi$ orbitals in N make a predominant contribution to the formation of the top part of the valence band. However, it is important to note that in addition to $2p_\pi$ orbitals in N, bonding orbitals 2p (N)−2sp^3 (Si) also contribute to the formation of the top part of the valence band. The overlap integral for $2p_\pi$ orbitals in nitrogen is small; for this reason, these orbitals correspond to heavy holes $m_h^* \approx 25m_0$ near the top of the valence band. Bonding orbitals 3sp^3(Si)−2p (N) near the top of the valence band correspond to light holes with $m_h^* \approx 0.5m_0$. These orbitals are characterized by large overlap integrals.

REFERENCES

1. V. A. Gritsenko, *Composition and Electronic Structure of Amorphous Insulators in Silicon-Based Metal−Insulator−Semiconductor Structures* (Nauka, Novosibirsk, 2003), p. 280 [in Russian].
2. V. A. Gritsenko, in *Silicon Nitride in Electronics* (Elsevier, New York, 1986), p. 263.
3. Y. Roizin and V. A. Gritsenko, in *Dielectric Films for Advanced Microelectronics*, Ed. by M. R. Baklanov, M. Green, and K. Maex (Wiley, New York, 2007), p. 486.
4. V. A. Gritsenko, K. A. Nasyrov, Yu. N. Novikov, A. L. Aseev, S. Y. Yoon, Jo-Won Lee, E.-H. Lee, and C. W. Kim, Solid-State Electron. **47**, 1651 (2003).
5. S.-H. Lee, K.-C. Park, and K. Kim, Appl. Phys. Lett. **87**, 073 510 (2005).
6. K. A. Nasyrov, S. S. Shaĭmeev, V. A. Gritsenko, J. H. Han, C. W. Kim, and J.-W. Lee, Zh. Éksp. Teor. Fiz. **129** (5), 926 (2006) [JETP **102** (5), 810 (2006)].
7. S.-Y. Ren and W. Y. Ching, Phys. Rev. B: Condens. Matter **23**, 5454 (1981).
8. Y.-N. Xu and W. Y. Ching, Phys. Rev. B: Condens. Matter **51**, 24 (1995).

sured at different excitation energies of 40.8, 200, 384, 620, and 1486.6 eV. The same figure shows the calculated photoelectron spectra of the valence band of α-Si_3N_4 obtained from the partial density of electron states with different symmetries of the wavefunctions taking into account the photoionization cross sections that depend on the excitation energy [35]. The posi-

NEKRASHEVICH et al.

9. A. Y. Liu and M. I. Cohen, Phys. Rev. B: Condens. Matter **41**, 10 727 (1990).

10. G. L. Zhao and M. E. Bachlechner, Phys. Rev. B: Condens. Matter **58**, 1887 (1998).

11. V. A. Gritsenko, Usp. Fiz. Nauk **178** (7), 727 (2008) [Phys.—Usp. **51** (7), 699 (2008)].

12. S. Miyasaki, Y. Ihara, and M. Hirose, Phys. Rev. Lett. **59**, 125 (1987).

13. V. A. Gritsenko, E. E. Meerson, and Yu. N. Morokov, Phys. Rev. B: Condens. Matter **57**, R2081 (1997).

14. T. P. Ma, IEEE Trans. Electron Devices **45**, 680 (1998).

15. Y.-C. Yeo, T.-J. King, and C. Hu, Appl. Phys. Lett. **81**, 2091 (2002).

16. K. A. Nasyrov, Yu. N. Novikov, V. A. Gritsenko, S. Y. Yoon, and C. W. Kim, Pis'ma Zh. Éksp. Teor. Fiz. **77** (7), 455 (2003) [JETP Lett. **77** (7), 385 (2003)].

17. K. A. Nasyrov, V. A. Gritsenko, Yu. N. Novikov, E.-H. Lee, S. Y. Yoon, and C. W. Kim, J. Appl. Phys. **96**, 4293 (2004).

18. K. A. Nasyrov, S. S. Shaimeev, V. A. Gritsenko, and J. H. Han, J. Appl. Phys. **105**, 123 709 (2009).

19. Y. C. Yeo, Q. Lu, W. C. Lee, T.-J. King, C. Hu, X. Wang, X. Guo, and T. P. Ma, IEEE Electron Dev. Lett. **21**, 540 (2000).

20. I.-H. Hong, T.-H. Lee, G.-C. Yin, D.-H. Wei, J.-M. Juang, T.-E. Dann, R. Klauser, T. J. Chuang, C. T. Chen, and K.-L. Tsang, Nucl. Instr. Methods Phys. Res., Sect. A **467**, 905 (2001).

21. S. Baroni, A. Dal Corso, S. de Gironcoli, and P. Giannozzi, http://www.pwscf.org/.

22. *ICSD 2003 Collection*, Entry No. 79798.

23. J. Robertson, Philos. Mag. B **63**, 47 (1991).

24. G. Pacchioni and D. Erbetta, Phys. Rev. B: Condens. Matter **60**, 12 617 (1990).

25. I. A. Brytov, Yu. N. Romashchenko, and V. A. Gritsenko, Zh. Éksp. Teor. Fiz. **89** (2), 562 (1985) [Sov. Phys. JETP **62** (2), 321 (1985)].

26. V. A. Gritsenko, Yu. N. Novikov, A. V. Shaposhnikov, and Yu. N. Morokov, Fiz. Tekh. Poluprovodn. (St. Petersburg) **35** (9), 1041 (2001) [Semiconductors **35** (9), 997 (2001)].

27. N. Lieske and R. Hezel, Thin Solid Films **61**, 217 (1979).

28. H. R. Philipp, J. Electrochem. Soc. **120**, 295 (1973).

29. D. L. Griscom, J. Non-Cryst. Solids **21**, 155 (1977).

30. G. M. Bartenev, S. M. Brekhovskikh, and A. Z. Varisov, Izv. Akad. Nauk SSSR, Neorg. Mater. **6**, 1553 (1970).

31. S. T. Pantelides and W. A. Harrison, Phys. Rev. B: Solid State **13**, 2267 (1976).

32. R. N. Nucho and A. Madhakar, Phys. Rev. B: Condens. Matter **21**, 1576 (1980).

33. E. P. O'Reilly and J. Robertson, Phys. Rev. B: Condens. Matter **27**, 3780 (1983).

34. S. Mukhopadhyay, P. V. Sushko, A. M. Stoneham, and A. Shluger, Phys. Rev. B: Condens. Matter **71**, 235 204 (2005).

35. J.-J. Yeh, *Atomic Calculation of Photoionization Cross-Section and Asymmetry Parameters* (Gordon and Breach, Amsterdam, 1993).

Translated by N. Wadhwa